Crown Segmentation From Computed Tomography Images With Metal Artifacts

Zeyang Xia, Yangzhou Gan, Jing Xiong, Qunfei Zhao, and Jie Chen

***Abstract*—Tooth segmentation from dental computed tomography (CT) images with metal artifacts is challenging as metal artifacts make some of the crown boundaries unrecognizable. This letter proposes a semiautomatic method for crown segmentation from CT images with metal artifacts. A user manually selects a starting slice and initializes this slice. Then crown contours are segmented automatically from volumetric CT images slice by slice. In the segmentation of each slice, the Radon transform is used to extract a line to separate neighboring crowns into independent ones. A statistical shape prior-based level set model is then applied to segment each crown from the mesial or distal side of the line. The proposed method was tested on 15 set of volumetric images. Experimental results validated that it is effective to extract crown contours from CT images with metal artifacts.**

***Index Terms*—Dental CT image, image segmentation, level set method, metal artifacts, statistical shape prior model.**

I. Introduction

THREE-DIMENSIONAL (3-D) digital models of the tooth are needed for computer-aided orthodontic treatment. Tooth segmentation is a fundamental work in reconstructing 3-D models from computed tomography (CT) images. During the past few decades, several automatic or semiautomatic segmentation methods have been reported. Akhoondali *et al.* [1] applied region growing method to segment teeth from other tissues. Heo *et al.* [2], [3] segmented the tooth contours using optimal threshold segmentation and B-spline fitting. Hiew *et al.* [4] used the graph-cut algorithm to interactively segment 3-D tooth volume. Hosntalab *et al.* [5] employed 3-D region-based level set method to extract tooth surfaces. Gao and Chae [6] proposed a level set model with shape and intensity prior to extract tooth contours. Yau *et al.* [7] and Ji *et al.* [8] used the similar model to segment tooth. Gan *et al.* [9] developed a hybrid level set model for the accurate segmentation of root.

However, these tooth segmentation methods were developed for images without metal artifacts. In clinics, patients in the middle of orthodontic treatment may need to be scanned while they have metal appliances (metal braces and arch wires) in their mouth. These metal appliances would result in streak-like artifacts which make some of the crown boundaries missing and unrecognizable.

This letter presents a novel method to address this challenging issue. Since the metal appliances are typically mounted on the crown so that the artifacts are restricted to the crown region only, the root contours are generally not affected. Thus, in this letter, we focused on the segmentation of crowns.

II. Crown Segmentation Method

The presented method segments the crown from the volumetric images semiautomatically. It starts from manually picking up a starting slice from tooth neck part and initializing each tooth in this slice. The initialization and segmentation of the starting slice are implemented using the method in [9]. Then, crown segmentation is completed automatically slice by slice. In the segmentation of each slice, the Radon transform is applied to extract a line to separate neighboring crowns into independent ones. Each crown is then individually segmented from the mesial or distal side of the line using a statistical shape prior-based level set model. Crown contour tracking strategy is employed to automatically initialize the crown contour using the segmented contour of previous slice.

A. Neighboring Crown Separation

As neighboring crowns may touch each other such that the common boundary in between is missing, segmentation algorithm may consider the two crowns as one and fail to separate them. To obtain individual crown contour, Gao and Chae [6] proposed to use coupled level set scheme. Although the coupled level set is effective to separate neighboring crowns, it is difficult to segment crowns from CT images with metal artifacts as each crown needs to be segmented separately by an individual level set to deal with the complex image condition.

Based on the assumption that neighboring crown contours can be completely separated by a straight line, this study utilizes the Radon transform to extract a line to separate neighboring

Manuscript received January 14, 2016; revised February 22, 2016; accepted March 16, 2016. Date of publication March 23, 2016; date of current version April 12, 2016. This work was supported by the National Natural Science Foundation of China under Grant 51305436 and 61403368, by the Guangdong Natural Science Funds for Distinguished Young Scholar Grant 2015A030306020, by the Major Project of Guangdong Province Science and Technology Department under Project 2014B090919002, and by the Shenzhen High-level Oversea Talent Program (Peacock Plan) Grant KQCX20130628112914284. The associate editor coordinating the review of this manuscript and approving it for publication was Prof. Arrate Munoz-Barrutia. *(Corresponding authors: Yangzhou Gan and Jing Xiong.)*

Z. Xia and Y. Gan are with the Shenzhen Institutes of Advanced Technology, Chinese Academy of Sciences, Shenzhen 518055, China, and also with the Key Laboratory of Human–Machine Intelligence-Synergy Systems, Chinese Academy of Sciences, Shenzhen 518055, China (e-mail: zy.xia@siat.ac.cn; yz.gan@siat.ac.cn).

J. Xiong is with the Shenzhen Institutes of Advanced Technology, Chinese Academy of Sciences, Shenzhen 518055, China (e-mail: jing.xiong@siat.ac.cn).

Q. Zhao is with the Shanghai Key Laboratory of Navigation and Location Services, and Department of Automation, Shanghai Jiao Tong University, Shanghai 200240, China (e-mail: zhaoqf@sjtu.edu.cn).

J. Chen is with the Department of Mechanical Engineering, Indiana University-Purdue University, Indianapolis, IN 46202 USA (e-mail: jchen3@iupui.edu).

Color versions of one or more of the figures in this letter are available online at http://ieeexplore.ieee.org.

Digital Object Identifier 10.1109/LSP.2016.2545702

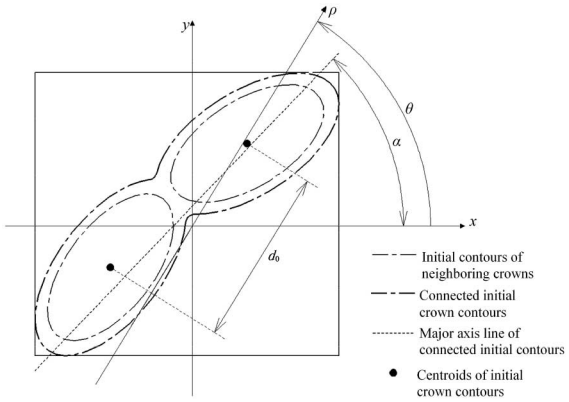

Fig. 1. Separation line of neighboring crowns corresponds to a local minimum $R(\theta_0, \rho_0)$ in the Radon transform.

crowns into independent ones such that each crown can be segmented independently. The Radon transform of a given image $I(x, y)(x, y \in \Re)$ represents a collection of one-dimensional (1-D) line integral (i.e., projection) in various directions

$$R(\theta, \rho)(I(x, y)) = \int_{-\infty}^{+\infty}\int_{-\infty}^{+\infty} I(x, y)\delta(\rho - x\cos\theta - y\sin\theta)\,dxdy \tag{1}$$

where θ denotes the angle between the perpendicular direction of line integral and the x-axis, and ρ denotes the perpendicular offset of the line integral.

The separation line of neighboring crowns corresponds to a local minimum point $R(\theta_0, \rho_0)$ in the Radon transform because the image projection along the separation line arrives a local minimum. The local minimum point $R(\theta_0, \rho_0)$ needs to satisfy two constraint conditions. 1) θ_0 should approximate to α, the angle of the major axis of the connected initial crown contours, such that the separation line remains approximately perpendicular to dental arch ($\theta_0 \in [\alpha - 20^0, \alpha + 20^0]$ in this study). 2) ρ_0 needs to be bounded within the perpendicular offset (d_0 in Fig. 1) of centroids of the initial contours. To speed up the calculation, the Radon transform was calculated within the minimal bounding rectangle of connected initial crown contours.

B. Crown Contour Segmentation

The metal artifacts with high intensity cover on partial region of crowns and make their boundaries missed and unrecognizable. It is difficult to obtain satisfying crown segmentation only using the underdetermined image information. This study applies the statistical shape prior-based level set model to extract the possible missed crown contours. The statistical shape prior-based models incorporate higher level prior knowledge about the shape of objects to help the segmentation algorithm extract the objects in the condition of underdetermined image information. It first learns the statistical shape prior model of crown to be segmented from a set of training samples and then incorporates this prior model into the level set curve evolution to constrain the curve evolving within a cluster of similar shapes.

1) Training Shapes Collection and Alignment: In this letter, two-dimensional (2-D) crown contours segmented manually from CT images of three subjects after the orthodontic treatment were used as the training set of crown shapes. There are no metal artifacts and tooth missing in these images. Since each jaw has 12–14 teeth symmetrically distributed in the left and right side, crown shapes in the training set are divided into seven groups according the tooth type.

Before constructing the statistical shape prior model, training shapes in each group need to be aligned to have the same position, scale, and direction. In this study, the shape alignment includes a mirroring operation and an affine transformation. The mirroring operation transforms crown shapes in the left and right side to the same side. The affine transformation involves three parameters T, s, and θ corresponding to translation, scale, and rotation, respectively. For any two shapes to be aligned, the three parameters can be obtained by the variation method [10] or Euclidean similarity transformation [11].

2) Dynamic Selection of Training Samples: From the tooth neck to the cusp of crown, the 2-D shapes of a same tooth differ a lot. Additionally, each group training set has more than one hundred samples. If all the samples are used to construct the shape prior model, there are too many redundant shapes which would reduce the accuracy and efficiency of the model. This study dynamically selects 30 training shapes to construct the statistical shape prior model. Given the initial contour of the crown to be segmented, samples with higher similarity with the initial contour have the priority to be the training shapes. Samples from the neighboring slice of the selected training shapes are also selected as the training shapes.

3) Constructing the Statistical Shape Prior Model: To construct the statistical shape prior model, the training shapes are represented implicitly and embedded into signed distance function (SDF). This study applies the Kernel density estimation to construct the statistical shape prior model [12], and the constructed model allows to approximate arbitrary distributions of shapes.

Given the set of training shapes $\{\Psi_i\}_{i=1,\ldots,n}$, the probability density of the shape Ψ on the space of SDF is defined by a Parzen–Rosenblatt kernel density estimator

$$p(\Psi) \propto \frac{1}{n}\sum_{i=1}^{n} \exp\left(-\frac{1}{2\sigma^2} d^2(\Psi, \Psi_i)\right) \tag{2}$$

where d^2 is the measure of shape distance, and σ is the kernel width. They are written as follows:

$$d^2(\Psi_1, \Psi_2) = \int_{\Omega_1} (H_\varepsilon(\Psi_1) - H_\varepsilon(\Psi_2))^2 dX \tag{3}$$

$$\sigma^2 = \frac{1}{n}\sum_{i=1}^{n} \min_{j \neq i} d^2(\Psi_i, \Psi_j) \tag{4}$$

where Ω_1 is the image domain of training shapes, $X \in \Re^2$ is a point in Ω_1, and H_ϵ is the normalized version of the Heaviside function [13].

The probability of shape Ψ on the subspace of the training shapes can be maximized by minimizing the following energy:

$$E(\Psi) = -\log p(\Psi). \tag{5}$$

The gradient descent flow of the above energy is written as

$$\frac{\partial \Psi}{\partial t} = \frac{\sum_{i=1}^{n} w_i \frac{\partial d^2(\Psi, \Psi_i)}{\partial \Psi}}{2\sigma^2 \sum_{i=1}^{n} w_i} \tag{6}$$

where w_i is the weight of force of training shape Ψ_i

$$w_i = \exp\left(-\frac{1}{2\sigma^2} d^2(\Psi, \Psi_i)\right). \tag{7}$$

4) Segmentation With the Statistical Shape Prior Model: In the conventional level set model, the zero-level set curve is driven under image force. For the model incorporated a statistical shape prior, a shape term E_S is introduced into the energy function to provide a force to drive the curve move toward the shape prior of a specific object. The energy of the level set model incorporated a shape prior is written as

$$E = E_I + \lambda E_S. \tag{8}$$

where E_I and E_S are the energy from the image data and shape prior, respectively, and $\lambda > 0$ is a positive weight parameter representing the contribution of the shape prior to the energy *E*.

In this study, the energy from the image data is defined as

$$E_I(\phi) = \int_{\Omega_2} g\delta_\varepsilon(\phi)|\nabla\phi| dX + \mu \int_{\Omega_2} \log\left(\frac{p(M_b|I(X))}{p(M_f|I(X))}\right) H_\varepsilon(\phi(X)) dX \tag{9}$$

where Ω_2 denotes the 2-D image plane, I: $\Omega_2 \to \Re$ denotes the gray level image, $\phi : \Omega_2 \to \Re$ denotes the level set function and takes positive and negative values inside and outside zero-level set curve, respectively, and δ_ϵ denotes the normalized Dirac delta function (derivation of H_ϵ).

In (9), the first term comes from the geodesic active contour model [14], and g denotes the edge detector. The second term represents region-based energy and is incorporated to deal with the split of crown contours, especially for molars.

Let $M = \{M_i | i = f, b\}$ denote the statistical model parameter of either the foreground or background, $p(M_i|I(X))$ is the posterior probability that a given point with intensity *I*(*X*) is the foreground or background. Given the foreground and background are equally likely, $p(M_i|I(X))$ is proportional to the prior conditional probability $p(I(X)|M_i)$. Assuming that the image intensity in the local region of the foreground and background is Gaussian distribution. The statistical parameters of Gaussian distribution are estimated from a narrow band (the band width is set to be five pixels) around the crown contour of the previous slice. In order to exclude possible outlier from the M_f model (foreground), only the pixels (empirically with CT numbers lower than 3000 HU) which are not corrupted by metal artifacts are considered in the calculation of $p(I(X)|M_f)$.

The energy from the shape prior is defined as the shape distance between the level set curve and shape prior model, and is expressed as

$$E_S = \int_{\Omega_2} (H_\varepsilon(\phi) - H_\varepsilon(\Psi))^2 dX. \tag{10}$$

Thus, the final energy of the level set model is written as

$$E(\phi) = \int_{\Omega_2} g\nabla\phi dX + \lambda \int_{\Omega_2} (H_\varepsilon(\phi) - H_\varepsilon(\Psi))^2 dX + \mu \int_{\Omega_2} \log\left(\frac{p(M_b|I(X))}{p(M_f|I(X))}\right) H_\varepsilon(\phi(X)) dX. \tag{11}$$

The above energy can be minimized using the following implicit gradient descent flow:

$$\frac{\partial \phi}{\partial t} = \text{div}\left(g\frac{\nabla\phi}{|\nabla\phi|}\right) - 2\lambda(H_\varepsilon(\phi) + H_\varepsilon(\Psi)) - \mu\delta_\varepsilon(\phi)\log\left(\frac{p(M_b|I)}{p(M_f|I)}\right). \tag{12}$$

The level set function ϕ and the statistical shape prior model Ψ are evolved alternatively based on gradient descent flow of (12) and (6), respectively [15]. The narrow band method [16] is applied for the evolution of the level set function and statistical shape prior model.

In this study, in order to prevent the level set reinitialization procedure, Gaussian filter was employed to regularize the level set function after each iteration. The Gaussian filter-based regularization not only smoothed the active contour but also eliminated the need for level set reinitialization [17].

III. Experiments

Cone beam CT (CBCT) images of 15 subjects treated with orthodontic arch wires were used to test the proposed method. CT images used for the training shape collection were not included in the tested images. These tested images were acquired by a CT scanner (NewTom VG, Italy) with 120 kV, 5 mA, a matrix of 624×624, a spatial voxel size of 0.25 mm, and the time of exposure of 6 s. All the images were scanned when the subjects' teeth were in an open bite position to make sure that the lower and upper teeth did not overlap in the images.

A. Qualitative Results

Fig. 2 presents the individual crown segmentation results on sample slices using the proposed method. It indicates that the extracted lines exactly separate neighboring crowns into independent ones, and missed crown boundaries are reconstructed and segmented successfully. The visual segmentation accuracy is satisfying.

Fig. 3 shows the qualitative comparison of different methods for segmenting the image in Fig. 2 (a)-1. Fig. 3(a)–(c) shows the results of Hosntalab's [5], Gao's [6], and Gan's [9] tooth segmentation methods. The results indicate that these methods fail to extract the crown boundaries occluded by metal artifacts with high intensity and get poor results.

B. Quantitative Results

The volumetric images of each subject were segmented manually by three experienced clinicians. A "gold standard" was constructed by combing the three manually segmentations using majority voting with equal weights and then compared to

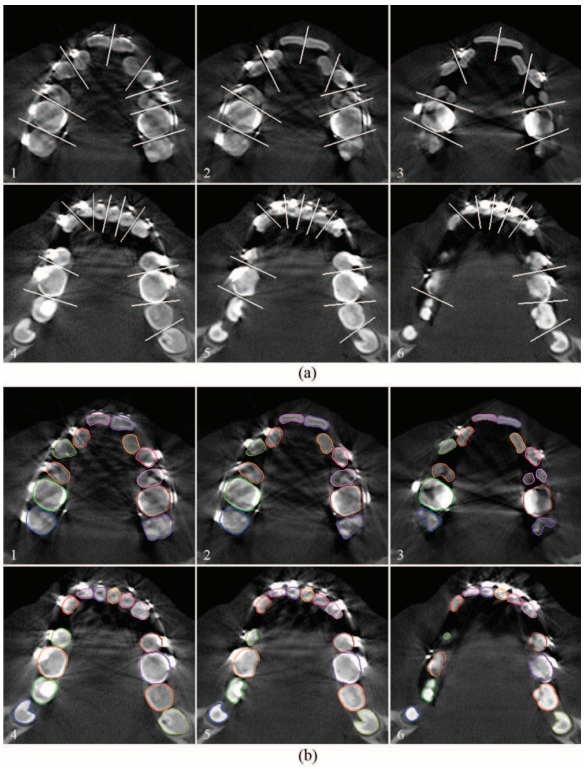

Fig. 2. Crown segmentation results on sample slices using the proposed method. (a) Neighboring crown separation line extraction results. (b) Crown contour segmentation results. The white lines denote the extracted separation line of neighboring crowns, and colored curves denote the segmented crown contours.

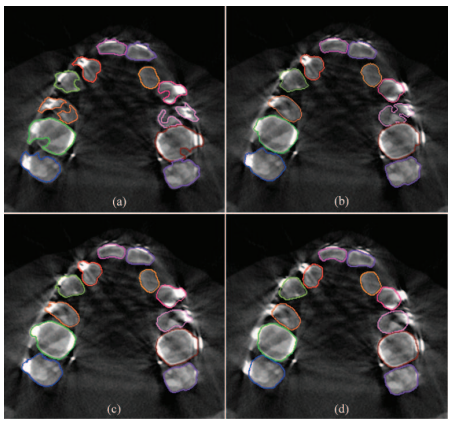

Fig. 3. Results comparison of different methods for segmenting the image in Fig. 2 (a)-1. (a)–(c) are the results using Hosntalab's [5], Gao's [6], and Gan's [9] methods, respectively. (d) is the manual segmentation results.

the results of algorithm. The dice similarity coefficient (DSC, %) and average symmetric surface distance (ASSD, mm) are used to quantitatively estimate the segmentation accuracy. DSC and ASSD are defined as

$$\mathrm{DSC} = \frac{2V_R \cap V_A}{V_R + V_A} \tag{13}$$

$$\mathrm{ASSD}(S_R, S_A) = \frac{\mathrm{mean}\left\{\mathrm{dist}\left(a, S_R\right), a \in S_A\right\} + \mathrm{mean}\left\{\mathrm{dist}\left(r, S_A\right), r \in S_R\right\}}{2} \tag{14}$$

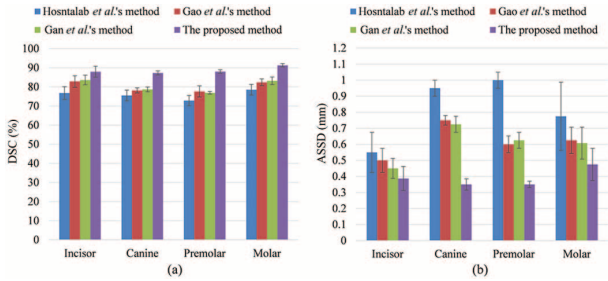

Fig. 4. Segmentation accuracy comparison of different methods. (a) DSC. (b) ASSD.

where V_R and V_A are the volumes of objects of gold standard and algorithm segmentation, respectively, S_R and S_A are the surfaces of objects of gold standard and algorithm segmentation, respectively, $\mathrm{dist}(a, S_R)$ is the nearest Euclidean distance from a point a to the surface S_R, mean$\{\bullet\}$ is the arithmetical average operator.

The quantitative segmentation accuracy of the proposed method and other three tooth segmentation methods for all the four types of teeth is presented in Fig. 4. The segmentation accuracy was estimated from slices of crown part. As the other three tooth segmentation methods were mainly developed for CT images without metal artifacts, they do not obtain satisfying crown segmentation for these tested images. Compared to these methods, the accuracy of the proposed method is higher. Statistical significance test showed that there was significant difference ($p < 0.01$) between the segmentation accuracy of the proposed method and the other three methods.

The main computation cost of the proposed method spends on the evolution of the level set function (14) and statistical shape prior model (6). For each iteration, the computational complexity is of the order O(kN) [15], where N is the number of grid points along the curve and k is the width of the narrow band. The proposed method was realized using MATLAB code and ran on a DELL graphic workstation (Win 7, Intel E5-2643 3.3-GHz CPU, 16-GB RAM). For the segmentation of the volumetric images of one subject, the user intervention procedure generally can be done within 30 s, and the automatic segmentation time was 5.36 ± 1.41 min. Compared to the manual segmentation which needs several hours, the efficiency is significantly improved.

IV. Conclusion

In this letter, a novel crown segmentation method from CT images with metal artifacts was proposed. This method segments crown contours from the volumetric images slice by slice. For the segmentation of each single slice, the Radon transform was first used to extract a line to separate neighboring crowns into independent ones. Then, a statistical shape prior-based level set model was applied to segment each crown from the mesial or distal side of the separation line. Experimental results on volumetric CT images of 15 subjects validated that the proposed method was effective to segment crowns from CT images with metal artifacts. In future, we will apply the proposed method to reconstruct 3-D models of the tooth for application of computer-aided orthodontic treatment diagnosis, planning, and simulation. It is also under consideration to apply the method in other similar applications.

REFERENCES

[1] H. Akhoondali, R. A. Zoroofi, and G. Shirani, "Rapid automatic segmentation and visualization of teeth in CT-scan data," *J. Appl. Sci.*, vol. 9, no. 11, pp. 2031–2044, 2009.

[2] H. Heo and O. S. Chae, "Segmentation of tooth in CT images for the 3D reconstruction of teeth," *Proc. SPIE*, vol. 5298, pp. 455–466, 2004.

[3] X. Wu *et al.*, "Improved B-spline contour fitting using genetic algorithm for the segmentation of dental computerized tomography image sequences," *J. Imag. Sci. Technol.*, vol. 51, no. 4, pp. 328–336, 2007.

[4] L. T. Hiew, S. H. Ong, and K. W. C. Foong, "Tooth segmentation from cone-beam CT using graph cut," in *Proc. Asia Pac. Signal Inf. Process. Assoc. Annu. Summit Conf. (APSIPA ASC)*, Biopolis, Singapore, 2010, pp. 272–275.

[5] M. Hosntalab, R. A. Zoroofi, A. A. Tehrani-Fard, and G. Shirani, "Segmentation of teeth in CT volumetric dataset by panoramic projection and variational level set," *Int. J. Comput. Assisted Radiol. Surg.*, vol. 3, no. 3–4, pp. 257–265, 2008.

[6] H. Gao and O. Chae, "Individual tooth segmentation from CT images using level set method with shape and intensity prior," *Pattern Recognit.*, vol. 43, no. 7, pp. 2406–2417, 2010.

[7] H. Yau, T. Yang, and Y. Chen, "Tooth model reconstruction based upon data fusion for orthodontic treatment simulation," *Comput. Biol. Med.*, vol. 48, pp. 8–16, May 2014.

[8] D. X. Ji, S. H. Ong, and K. W. C. Foong, "A level-set based approach for anterior teeth segmentation in cone beam computed tomography images," *Comput. Biol. Med.*, vol. 50, pp. 116–128, Jul. 2014.

[9] Y. Gan, Z. Xia, J. Xiong, Q. Zhao, Y. Hu, and J. Zhang, "Towards accurate tooth segmentation from computed tomography images using a hybrid level set model," *Med. Phys.*, vol. 42, no. 1, pp. 14–27, Jan. 2015.

[10] N. Paragios, M. Rousson, and V. Ramesh, "Matching distance functions a shape to area variational approach for global-to-local registration," in *Proc. ECCV*, Copenhagen, Denmark, 2002, pp. 775–789.

[11] M. B. Stegmann and D. D. Gomez, *A Brief Introduction to Statistical Shape Analysis*. Kongens Lyngby, Denmark: Informatics and Mathematical Modelling, Technical University of Denmark, DTU, Mar. 2002.

[12] D. Cremers, S. Osher, and S. Soatto, "Kernel density estimation and intrinsic alignment for shape priors in level set segmentation," *Int. J. Comput. Vis.*, vol. 69, no. 3, pp. 335–351, May 2006.

[13] T. F. Chan and L. A. Vese, "Active contours without edge," *IEEE Trans. Image Process.*, vol. 10, no. 2, pp. 266–277, Feb. 2001.

[14] V. Caselles, R. Kimmel, and G. Sapiro, "Geodesic active contours," *Int. J. Comput. Vis.*, vol. 22, no. 1, pp. 61–79, Jan. 1997.

[15] W. Liu, Y. Shang, X. Yang, R. Deklerck, and J. Cornelis, "A shape prior constraint for implicit active contours," *Pattern Recognit. Lett.*, vol. 32, no. 15, pp. 1937–1947, 2011.

[16] D. Adalsteinsson and J. A. Sethian, "A fast level set method for propagating interfaces," *J. Comput. Phys.*, vol. 118, no. 2, pp. 269–277, 1995.

[17] K. Zhang, H. Song, and L. Zhang, "Active contours driven by local image fitting energy," *Pattern Recognit.*, vol. 43, no. 4, pp. 1199–1206, Apr. 2010.